Nonparabolicity and a sum rule associated with bound-to-bound and bound-to-continuum intersubband transitions in quantum wells

Carlo Sirtori, Federico Capasso, and Jérôme Faist
AT&T Bell Laboratories, Murray Hill, New Jersey 07974

Sandro Scandolo
International School for Advanced Studies, Via Beirut 4, I-34014 Trieste, Italy
(Received 5 May 1994)

A sum rule for electronic intersubband transitions has been derived following Kane's model, beyond the quadratic dispersion relations. The sum rule takes into account the effects of nonparabolicity and the different effective masses in the well and barrier materials; it depends on the property of the ground state of the system and, as such, on the shape of the potential. The boundaries of the validity of matrix element computations are also discussed in the case where only the conduction band is included. Experimental results are presented for bound-to-bound and bound-to-continuum intersubband transitions in various types of $Al_{0.48}In_{0.52}As/Ga_{0.47}In_{0.53}As$ quantum well systems (single wells, coupled wells, and quantum wells with Bragg confinement); the agreement with theory is excellent. In the last section of the paper, the effect of the electric field on the sum rule is investigated.

I. INTRODUCTION

Optical transitions between electronic states within the conduction band of doped semiconductor heterostructures have recently proved to be promising candidates for the realization of infrared photodetectors,[1] frequency converters,[2] and lasers,[3] and a large effort has been devoted to the investigation of both the linear and the nonlinear optical properties of these systems. Particular attention has been paid to heterostructures with large values of the conduction-band offset ($\Delta E_c \geq 300$ meV) due to the possibility of achieving higher transition energies. Experimental observation of "high-energy" intersubband transitions in quantum wells has been reported for strained[4] and lattice-matched[5] $Ga_yIn_{1-y}As/Al_xIn_{1-x}As$, GaAs/AlAs,[6] and strained $In_yGa_{1-y}As/Al_xGa_{1-x}As$ (Ref. 7) systems.

Theoretical predictions of the electronic energies and of the optical transition strengths have been mainly based on standard one-band envelope-function Hamiltonians. While this is certainly a good approximation for energy levels located near the bottom of the conduction band, as soon as the confinement energy becomes comparable with the interband energy gap, the full valence- and conduction-band structure has to be taken into account . Although this is still an approximation (the whole band structure of the bulk material should be considered in order to obtain exact results within the envelope-function approximation), this model, also referred to as the Kane model,[8] has been shown to work rather well in the cases of interest. Its only drawback is the increase in the computational effort and the loss of a "textbook" picture which instead characterizes one-band Hamiltonians.

It has been recently proposed,[9] however, that the four-band Kane model can be reduced, as long as electron (conduction) states are considered, to an "effective" two-band model, which can in turn be recast into a one-band model, provided an appropriate energy dependence is given to the effective mass, thus recovering the use of textbook Hamiltonians. Although electron energies calculated using this simple model turn out to be in excellent agreement with the observed values, complications arise when the optical properties of these systems are considered.[10] In fact, it can be shown that the standard procedure for calculating the optical transition strengths between electron states of a quantum well is inapplicable in the presence of nonparabolicity effects, and that a more refined theory is required. The first aim of this paper is to compare the predictions of this theory with experimental results obtained in $Ga_{0.47}In_{0.53}As/Al_{0.48}In_{0.52}As$ multiple quantum wells ($\Delta E_c \simeq 510$ meV).

The issue of sum rules for the integrated intersubband absorption will also be addressed. Sum rules for the integrated intraband absorption have a long history. Sommerfeld and Bethe[11] first pointed out that the sum of the oscillator strengths for optical transitions inside the conduction band of a metal (the Drude absorption) is simply given by m_0/m^*, where m^* is the effective mass of the conduction band. It was later recognized by Lax[12] that the same sum rule also applies to transitions between shallow-impurity states in semiconductors. Here we generalize the intraband sum rule to include the effects of nonparabolicity and we report its experimental verification in semiconductors. We also observe, as expected, the invariance of the sum rule upon introduction of an external electric field.

The work is organized as follows. In Sec. II we show how reliable schemes for calculating energy levels can be constructed starting from the well-known four-band Kane model. These schemes allow in a natural way the

0163-1829/94/50(12)/8663(12)/$06.00

presence of nonparabolicity effects. In Sec. III we develop, within these models, a theory for the intersubband optical transitions which overcomes the inconsistencies of the standard theory in the nonparabolic case. In Sec. IV we derive a sum rule for the integrated value of the absorption coefficient. Experimental confirmations of these predictions are presented in detail in Sec. V.

II. ENERGY LEVELS

We start by considering the envelope-function Hamiltonian in the Kane approximation.[8] The in-plane momentum is assumed to vanish. As is well known, in this case the heavy-hole state is decoupled from the original 4×4 Hamiltonian (8×8 reduced by spin degeneracy), and we are left with the following 3×3 Hamiltonian:

$$\mathcal{H} = \begin{pmatrix} E_c(z) & \sqrt{\frac{2}{3}}\frac{p_{cv}}{m_0}p_z & -\sqrt{\frac{1}{3}}\frac{p_{cv}}{m_0}p_z \\ -\sqrt{\frac{2}{3}}\frac{p_{cv}}{m_0}p_z & E_{lh}(z) & 0 \\ \sqrt{\frac{1}{3}}\frac{p_{cv}}{m_0}p_z & 0 & E_{\rm so}(z) \end{pmatrix} \quad (1)$$

acting on the three-dimensional vector of envelope functions $\psi = (\phi_c, \phi_{\rm lh}, \phi_{\rm so})$, where c, lh, and so label conduction, light-hole, and split-off position-dependent band edges, respectively. The momentum matrix element p_{cv} between bulk Bloch states can be also written as $p_{cv} = i\sqrt{m_0 E_p/2}$, where E_p is the Kane energy ($\sim$ 20 eV in III-V semiconductors). Notice that we are neglecting the diagonal "free-electron" term $p_z^2/2m_0$, which can be shown to contribute only with terms of order $(E_c - E_{\rm lh,so})/E_p \ll 1$. If we are only interested in the energy levels located above the edge of the conduction band, the problem can be solved using the second and third rows of (1) to express the equation in the first row as

$$p_z \frac{1}{2m(E,z)} p_z \phi_c + E_c(z)\phi_c = E\phi_c \quad (2)$$

with the energy- and position-dependent effective mass

$$\frac{1}{m(E,z)} = \frac{1}{m_0}\left[\frac{2}{3}\frac{E_p}{E - E_{\rm lh}(z)} + \frac{1}{3}\frac{E_p}{E - E_{\rm so}(z)}\right] . \quad (3)$$

The solutions of the differential equation (2) give the conduction component ϕ_c and the energy of the stationary states. We must recall, however, that the total stationary wave function is given by the three components ϕ_c, $\phi_{\rm lh}$, and $\phi_{\rm so}$, weighted with their corresponding Bloch functions, so that the only knowledge of the conduction component is insufficient for the complete physical description of the stationary state. Moreover, while the total Hamiltonian operator (1) is Hermitian, its restriction (2) to the conduction component is not Hermitian due to the energy dependence of the mass.[13] Therefore Eq. (2) cannot be assumed, alone, as a Schrödinger equation of the system. For example, Eq. (2) does not guarantee either completeness or orthogonality of its eigenfunction set.[10]

Nonparabolicity effects have been also introduced through a k^4 dependence of the electron Hamiltonian (and a constant effective mass),[14–16] with appropriate boundary conditions for the wave functions.[15] The controversy on the equivalence of the two approaches has been finally resolved[16] and tested numerically with a transfer-matrix method.[17]

As far as electron states are considered [we define electron states as all those states whose energy E exceeds the minimum of the conduction-band edge $E_c(z)$], the three-band model can be further simplified through a unitary transformation which allows one to replace light-hole and split-off bands with an "effective" valence band v. As shown in the Appendix, the resulting 2×2 Hamiltonian acting on the two-component wave function (ϕ_c, ϕ_v) is given by

$$\mathcal{H} = \begin{pmatrix} E_c(z) & \frac{p_{cv}}{m_0}p_z \\ -\frac{p_{cv}}{m_0}p_z & E_v(z) \end{pmatrix} , \quad (4)$$

where $E_v = (2E_{\rm lh} + E_{\rm so})/3$. Electron energies and wave functions will differ from those obtained using (1) by terms of order $(\Delta/|E_c - E_v|)^2$, with $\Delta = \sqrt{2}(E_{\rm lh} - E_{\rm so})/3$. For typical III-V semiconductors this factor is quite small; in GaInAs, for example, we have $(\Delta/|E_c - E_v|)^2 \simeq 0.04$.[18] We stress, however, that this effective band is a pure formal artifact which cannot be used to describe, for example, the hole states of the system.

Similarly to what has been done in the 3×3 case, we obtain from (4) the differential equation (2), where now the energy-dependent effective mass is simply given by

$$m(E,z) = m_0 \frac{E - E_v(z)}{E_p} . \quad (5)$$

While a two-band model simply obtained neglecting the split-off component[19] has been shown to be too crude an approximation,[17] the improvement obtained by this effective valence-band model is remarkable. In the empirical approach of Ref. 9, the parameters $E_c - E_v$ and E_p are determined from measured values of $m^* = m(E = E_c)$ of the constituent materials and from the knowledge of their nonparabolicity coefficient, defined as $\gamma^{-1} = 2m^*|E_c - E_v|/\hbar^2$. Moreover, since in the envelope-function approximation the value of E_p is taken to be the same in the well and and in the barrier,[20] only the knowledge of m^* is required for the barrier material. Equivalently, one could choose, instead of γ, the measured value of $|E_c - E_v|$, and determine E_p through the knowledge of m^*. Although the two methods yield slightly different values of E_v and E_p, they are both correct within the two-band approximation, provided the mutual relationships $\gamma m^*|E_c - E_v| = \hbar^2/2$ and $m^* = E_p/|E_c - E_v|$ are maintained.

In the specific case of our GaInAs/AlInAs quantum wells, calculations have been performed following Nelson *et al.*,[9] i.e., using m^* and γ as input parameters. For the GaInAs wells their values are $m^* = 0.043m_0$, and $\gamma = 1.13 \times 10^{-14}$ cm^2; for the AlInAs barriers $m^* = 0.072m_0$. These parameters give a Kane energy

$E_p = 18.3$ eV and an effective energy gap $|E_c - E_v| = 0.79$ eV, which are in fair agreement with the tabulated values[18] $E_p = 21.9$ eV and $|E_c - E_v| = 0.93$ eV [we recall that $E_v = (2E_{\rm lh} + E_{\rm so})/3$]. Vice versa, the use of the tabulated E_p and $|E_c - E_v|$ as input parameters would yield the same value for m^* but a slightly smaller value of the nonparabolicity coefficient, $\gamma = 0.95 \times 10^{-14}$ cm^2. The reason for the choice of the method of Nelson *et al.* is that the experimental values of m^* and γ are in principle determined by the whole band structure, and they could therefore introduce phenomenologically the effects of remote bands in the Kane formulation. Moreover, equal masses and slightly different nonparabolicity coefficients do not alter qualitatively the calculated energies. Finally, the conduction-band offset has been fixed at 0.51 eV.

III. OPTICAL TRANSITIONS

Optical transitions between stationary states of a system are commonly described in terms of oscillator strengths f, defined as

$$f_{0i} = \frac{2}{m_0} \frac{|\langle \psi^{(0)} | \mathcal{P} | \psi^{(i)} \rangle|^2}{E_i - E_0}, \tag{6}$$

where $\psi^{(0)}$ and $\psi^{(i)}$ are stationary states and $\mathcal{P}$ is the momentum operator. In the matrix notation adopted in the preceding section, the momentum operator $\mathcal{P}$ corresponding to the Kane Hamiltonian (1) is given by[8]

$$\mathcal{P} = \begin{pmatrix} 0 & \sqrt{\frac{2}{3}} p_{cv} & -\sqrt{\frac{1}{3}} p_{cv} \\ -\sqrt{\frac{2}{3}} p_{cv} & 0 & 0 \\ \sqrt{\frac{1}{3}} p_{cv} & 0 & 0 \end{pmatrix} . \tag{7}$$

In order to be consistent with Hamiltonian (1), where the free-electron term was neglected, we have dropped the diagonal p_z term in the momentum matrix. Although many attempts to deal with the nonparabolicity problem made use of Eq. (2) to correctly determine energy eigenvalues, the relevance of the valence components in the evaluation of oscillator strengths has never been stressed, except in the work by Leavitt,[10] where the problem is correctly examined, although in an empirical two-band model. In the following we will extend his results to the full three-band Kane model. In particular, the standard use of dipole matrix elements $\langle z \rangle$ between the solutions of (2) (our conduction components) is not justified for at least two reasons. First, conduction components belonging to different stationary states are not orthogonal functions, so that dipole matrix elements between them are ill-defined. Second, in the one-dimensional subspace of the conduction component, any expression of the type $[H, z] = ip_z/m$ [which is required to express (6) in terms of dipole moments] is meaningless due to the energy dependence of m. Therefore, nonparabolicity corrections to the oscillator strengths cannot formally be accounted for using dipole moment matrix elements between conduction components. As a matter of fact, however, empirical procedures based on the orthogonalization of excited states provide results which are comparable to the correct ones within experimental accuracy.

The correct procedure for calculating oscillator strengths must be derived from their exact definition to be free of inconsistencies. In principle, one should solve Eq. (2), derive light-hole and split-off components making use of (1), and evaluate oscillator strengths with the use of (7). In practice, one can show, after some algebra, that the momentum matrix element in (6) is simply related to the conduction components of the total wave function as

$$\langle \psi^{(0)} | \mathcal{P} | \psi^{(i)} \rangle = \frac{1}{2} \left\langle \phi_c^{(0)} \left| p_z \frac{m_0}{m(E_0, z)} + \frac{m_0}{m(E_i, z)} p_z \right| \phi_c^{(i)} \right\rangle , \tag{8}$$

with $m(E)$ given by (3). An alternative form for the oscillator strength expressed in terms of appropriate dipole-moments can also be derived starting from (6). In fact, if one defines a dipole-moment *matrix* as

$$\mathcal{Z} = \begin{pmatrix} z & 0 & 0 \\ 0 & z & 0 \\ 0 & 0 & z \end{pmatrix} , \tag{9}$$

it is straightforward to show that $\mathcal{Z}$ satisfies the well-known commutation relation

$$\mathcal{P} = \frac{im_0}{\hbar} [\mathcal{H}, \mathcal{Z}] . \tag{10}$$

Notice that, unlike the single matrix element $\langle \phi_c | z | \phi_c \rangle$, $\mathcal{Z}$ is not ill-defined, due to the orthogonality of the total wave function. Inserting (10) into (6), we obtain

$$f_{0i} = \frac{2m_0}{\hbar^2} (E_i - E_0) |\langle \psi^{(0)} | \mathcal{Z} | \psi^{(i)} \rangle|^2 . \tag{11}$$

Although the dipole-moment expectation value in (11) can be useful for making comparisons with experimental results, it is worth stressing that expression (11) may not be defined in infinite systems. Moreover, expression (8) only requires the knowledge of the solutions of (2), and not of the full wave function, as in (11). In using (8), however, one must recall that ϕ_c is a solution of (2) normalized so that

$$\langle \phi_c | \phi_c \rangle + \langle \phi_{\rm lh} | \phi_{\rm lh} \rangle + \langle \phi_{\rm so} | \phi_{\rm so} \rangle = \langle \phi_c | 1 + \tfrac{2}{3} p_z \frac{|p_{cv}|^2/m_0^2}{[E^{(i)} - E_{\rm lh}(z)]^2} p_z + \tfrac{1}{3} p_z \frac{|p_{cv}|^2/m_0^2}{[E^{(i)} - E_{\rm so}(z)]^2} p_z | \phi_c \rangle = 1 . \tag{12}$$

It is straightforward to check that in the limit of $|E_c - E_{\rm lh,so}| \gg E - E_c$ the standard effective-mass treatment of the intersubband transitions is recovered. We first notice that in this limit $m(E_i, z) \simeq m(E_0, z) \simeq m^*(z)$. We also observe that the additional expectation values in (12) vanish, so that $\langle \phi_c | \phi_c \rangle = 1$. We then write down explicitly the oscillator strength (6) using (8) and we obtain, as expected,

$$f_{0i} = \frac{m_0}{2} \frac{|\langle \phi_c^{(0)}| \left[p_z m^*(z)^{-1} + m^*(z)^{-1} p_z \right] |\phi_c^{(i)}\rangle|^2}{E_i - E_0}, \quad (13)$$

or, in terms of dipole moments, as

$$f_{0i} = \frac{2m_0}{\hbar^2}(E_i - E_0)|\langle \phi_c^{(0)}|z|\phi_c^{(i)}\rangle|^2. \quad (14)$$

The scaled oscillator strength $f' = (m^*/m_0)f$ is also commonly defined in the literature in connection with the sum rule which will be discussed in the following sections. It must be observed, however, that the dependence of m^* on the position does not allow one to extract m^* out of the expectation value in (13), nor to multiply it as an external factor, unless the same effective mass is chosen for different materials.[21]

We now turn our attention to the two-band model and we examine how optical transitions can be described in this model. The unitary transformation adopted in the preceding section to simplify the three-band model gives for the momentum matrix

$$\mathcal{P} = \begin{pmatrix} 0 & p_{cv} \\ -p_{cv} & 0 \end{pmatrix}, \quad (15)$$

as shown in the Appendix.

It is straightforward to show that the momentum matrix elements in the two-band model agree with expression (8), provided the form (5) is chosen for the effective mass, as shown also by Leavitt.[10] Again, the conduction component must be normalized in such a way that

$$\langle \phi_c | 1 + T^{(i)} | \phi_c \rangle = 1 \quad (16)$$

with

$$T^{(i)} = \frac{1}{2m(E^{(i)}, z)[E^{(i)} - E_v(z)]} p_z^2 = \frac{E^{(i)} - E_c(z)}{E^{(i)} - E_v(z)}. \quad (17)$$

Notice that the expectation value of $T^{(i)}$ is proportional to the kinetic energy of the considered state, and is therefore a positive quantity.

In Fig. 1 we show the theoretical results obtained for the $0 \rightarrow 1$ transition in an AlInAs/GaInAs single quantum well of variable width, expressed as a function of the ground-state energy. The oscillator strengths calculated with our procedure (solid line) are compared with those obtained from the *standard* dipole-moment technique (dotted line). Although the dipole moment is in general ill-defined due to nonorthogonality, in *symmetric* structures the orthogonality of different wave functions is restored by parity. As can be seen, the standard dipole procedure typically overestimates the exact result only by about 5–10%. A systematic reduction of the observed oscillator strengths with respect to the calculated ones has indeed been reported in many experimental works. In *asymmetric* structures, the unphysical dependence of the dipole matrix elements on the choice of the origin is commonly overcome by imposing the excited-state wave functions to be orthogonal to the ground state. Since this empirical procedure has always shown good agreement with the experimental data, we may argue that the appropriate use of standard dipole moments still provides acceptable results.

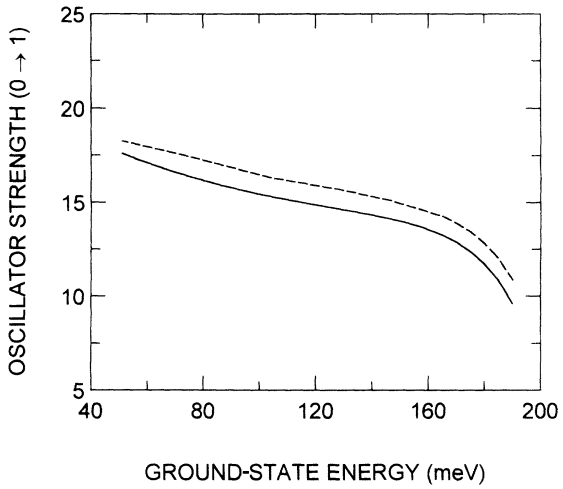

FIG. 1. Oscillator strength of the $0 \rightarrow 1$ transition for a GaInAs/AlInAs single quantum well of variable width, as a function of the ground-state energy, calculated using Eq. (6) (solid line), and using the standard dipole-moment technique (dashed line).

IV. *f*-SUM RULE

While it has been known since the dawn of quantum mechanics that the *total* sum of the oscillator strengths is unity[22] regardless of the details of the system, the problem of evaluating *partial* sums of oscillator strengths has always attracted considerable interest,[23] due to the limited portion of the spectrum accessible to standard spectroscopic techniques. As far as metals are concerned, for example, a clear physical distinction can be made between transitions involving free and bound electrons, the latter requiring much larger photon energies than the former. The m_0/m^* sum rule found by Sommerfeld and Bethe for intraband transitions in metals was then extended by Lax[12] to shallow impurities states in semiconductors, where the ratio m_0/m^* typically exceeds unity by more than one order of magnitude. Extensions of the Lax sum rule have been recently reported by Peeters *et al.*[24] in the case of superlattices, and by Davé and Taylor[25] in the case of a position-dependent effective mass.

Both the Sommerfeld-Bethe and the Lax results rely on Bloch's idea that electrons located at the extrema of a band respond to large-scale perturbations as particles with a scaled effective mass given by the curvature of the corresponding band extremum. As soon as the parabolic-band picture of the electron dynamics fails, as in our case, the previously established intraband sum rules lose their validity. In this section we are going to present a new sum rule for the oscillator strengths of intraband transitions in semiconductors which includes the effects of band nonparabolicity.

We start by defining the quantity S as

$$S = \sum_i f_{0i} \ , \tag{18}$$

where f_{0i} has been defined in (6) and i runs over all eigenstates of the Hamiltonian (1) or (4). The quantity S can be simply evaluated using the same procedure adopted for the evaluation of the f-sum rule,[22] namely,

$$\begin{aligned} S &= \frac{2}{m_0} \sum_i \frac{\langle \psi^{(0)}|\mathcal{P}|\psi^{(i)}\rangle\langle\psi^{(i)}|\mathcal{P}|\psi^{(0)}\rangle}{E^{(i)} - E^{(0)}} \\ &= -\frac{i}{\hbar} \sum_i \langle \psi^{(0)}|[\mathcal{Z},\mathcal{P}]|\psi^{(0)}\rangle = 0 \ , \end{aligned} \tag{19}$$

since $[\mathcal{Z},\mathcal{P}] = 0$, as can be obtained from their definitions. The same conclusions can be reached in the two-band model, provided the two-dimensional analog of (9) is considered.

We must pay attention to the fact that we have summed over *all* the eigenstates of the system, i.e., also over valence states (which, in this context, can be defined as states with energy $E < E_v$). In spite of the fact that transitions to valence states are essential to formally obtain the result in (19), as a matter of fact all the valence states are filled, so that transitions to them are not allowed by the Pauli exclusion principle. As a consequence, only those states which lie higher in energy from the ground state ψ_0 can be experimentally observed. By splitting the sum into allowed (intraband) and forbidden (interband) terms as follows:

$$\sum_{i \text{ allowed}} f_{0i} + \sum_{i \text{ forbidden}} f_{0i} = S_a + S_f = 0 \ , \tag{20}$$

we immediately argue that the sum over the forbidden interband transitions is given by the opposite of the sum over the observed intraband transitions. Since the oscillator strengths to valence states are negative [due to the energy denominator in (6)], the sum over the allowed transitions is greater than zero, as expected. This enhancement effect due to the Pauli principle is also well known to occur, for example, in alkali metals,[26] although on a smaller scale. In other words, forbidden interband transitions can be viewed, within this framework, as the physical origin of the strong $\simeq m_0/m^*$ enhancement of intraband transitions.

Incidentally, since the Hamiltonian (4) is formally equivalent to the Dirac relativistic Hamiltonian for the electron[27] (providing that $p_{cv}/m_0 \to c$ and $m^* \to 2m_0$), our sum rule (19) coincides with the results of Levinger *et al.*,[28] who obtained a vanishing sum rule for the Dirac Hamiltonian on the basis of its linear dependence on the momentum. In other words, the well-known total f-sum rule of linear optics can be seen to arise, as in our case, from the contribution due to forbidden transitions to filled electron states with negative energy (empty positrons).

Using Eq. (20), we now give an estimate of the sum rule S_a for intraband transitions in the general case where nonparabolicity effects are not negligible. For sake of simplicity, we adopt here the effective two-band model. We also make the simplifying assumption that conduction and valence bands display a "specular" band alignment, i.e., that they are just mirror images with respect to the center of the gap. This assumption is not exact in general, since it depends on the specific choice of the conduction-band offsets,[29] but yields, as we will see, to a very simple expression for S_a. This expression will be finally compared with the exact sum of the intraband oscillator strengths to establish its degree of accuracy.

The sum rule for the allowed transitions can be written, using the total sum rule as

$$S_a = -S_f = -\frac{2}{m_0} \sum_v \frac{|\langle \psi^{(0)}|\mathcal{P}|\psi^{(v)}\rangle|^2}{E^{(v)} - E^{(0)}} \ , \tag{21}$$

where v runs over all valence states. A specular band alignment for conduction and valence bands implies that once the conduction states $\psi^{(c)}$ are obtained, the valence states $\psi^{(v)}$ can be simply derived exchanging the two components of the conduction state as follows:

$$\psi^{(v)} \equiv (\phi_c^{(v)}, \phi_v^{(v)}) = (\phi_v^{(c)}, \phi_c^{(c)}) \ . \tag{22}$$

Using (15) and (22) we obtain

$$\langle \psi^{(0)}|\mathcal{P}|\psi^{(v)}\rangle = \delta_{0,v} p_{cv} \left[\langle \phi_c^{(0)}|\phi_c^{(0)}\rangle - \langle \phi_v^{(0)}|\phi_v^{(0)}\rangle\right] \ , \tag{23}$$

where the Kronecker δ arises from neglecting nonorthogonality between conduction components (calculated overlaps never exceed 5% in our systems). The sum over v in Eq. (21) is therefore restricted to the single term

$$S_a = \frac{2}{m_0} \frac{|p_{cv}|^2 \left[\langle \phi_c^{(0)}|\phi_c^{(0)}\rangle - \langle \phi_v^{(0)}|\phi_v^{(0)}\rangle\right]^2}{E^{(0)} - E^{(0,v)}} \ , \tag{24}$$

where $E^{(0,v)}$ is the energy of the valence ground state. In the case of specular alignment $E^{(0,v)}$ would just be given by $E_v - (E^{(0)} - E_c)$. However, as a crude attempt to take into account the actual nonspecular alignment (valence-band offsets are typically smaller than conduction-band offsets in III-V semiconductors) we force the valence-ground-state confinement energy not to exceed the value of the valence-band offset ΔE_v, i.e., we set

$$E_v - E^{(0,v)} = \min(E^{(0)} - E_c, \Delta E_v) \ , \tag{25}$$

where the band-edge energies E_c and E_v refer to the well material and $\Delta E_v = 20$ meV in our case. Notice that this value of the band offset refers to the band alignment of the effective valence bands, and bears no relationship with the real valence-band offset. Since conduction and valence components of the conduction ground state can be related, using (4), as

$$\phi_v^{(0)} = -\frac{p_{cv}}{m_0} \frac{1}{E^{(0)} - E_v} p_z \phi_c^{(0)} \ , \tag{26}$$

we also have

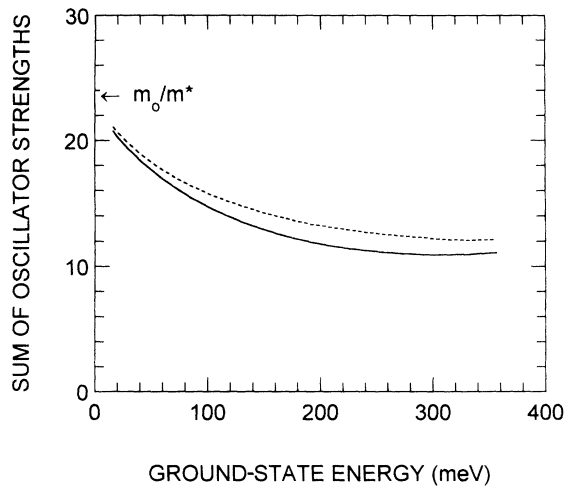

FIG. 2. Sum of the oscillator strengths for a GaInAs/AlInAs single quantum well of variable well width, as a function of the ground-state energy. The solid line refers to the sum rule (27), the dotted line refers to the exact result obtained using Eq. (6), and m_0/m^* indicates their limit value for infinite well widths.

$$S_a = |\langle \phi_c^{(0)}|1 - T^{(0)}|\phi_c^{(0)}\rangle|^2 \frac{E_p}{E^{(0)} - E^{(0,v)}} \qquad (27)$$

with $T^{(0)}$ given by (17). Expression (27) predicts a significant reduction of the overall absorption in the presence of nonparabolicity effects due both to the enhancement of the energy denominator and to the reduction of the "kinetic" $\langle 1 - T \rangle$ factor. This result is obviously consistent with the reduction of the single $0 \rightarrow 1$ transition discussed in the preceding section.

In Fig. 2 we report the computed values of expression (27) (solid line) for AlInAs/GaInAs single quantum wells as a function of the ground-state energy. For sufficiently thin wells (large ground-state energies) the sum rule shows a dramatic reduction of the optical transitions with respect to the parabolic infinite-well case m_0/m^*, with m^* given by the well material (in our formalism the parabolic case is obtained as the limit $E - E_c \ll E_c - E_v$, which implies that the wave function is completely confined in the well material). To test the accuracy of our sum rule, we also display the sum of the oscillator strengths calculated term by term using (6) and (8) (dotted line). The agreement between the sum rule and the exact calculation is fairly good. Notice that around 200 meV a drastic change occurs in the absorption spectrum due to the transition from a dominantly bound-to-bound regime to a bound-to-continuum regime, the first excited state becoming unbound around this value of the ground-state energy. In spite of this, the sum rule follows with good accuracy the exact value of the total absorption strength and they both show no particular feature. This

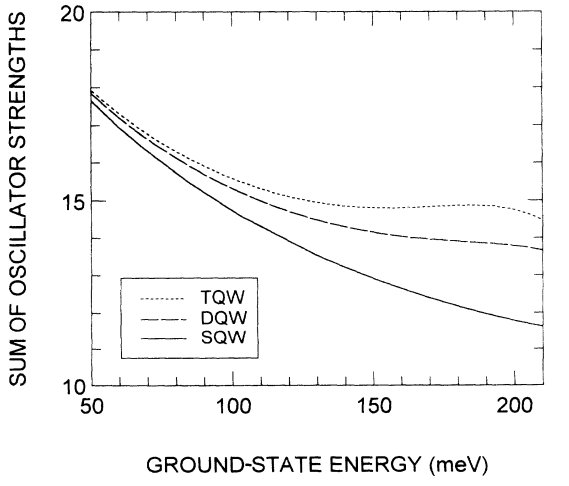

FIG. 3. Sum of the oscillator strengths calculated using the sum rule (27) for three different quantum well structures: single (SQW), double (DQW), and triple quantum well (TQW). The sum is plotted vs the ground-state energy, where the ground-state energy is varied by varying the width of the thickest well.

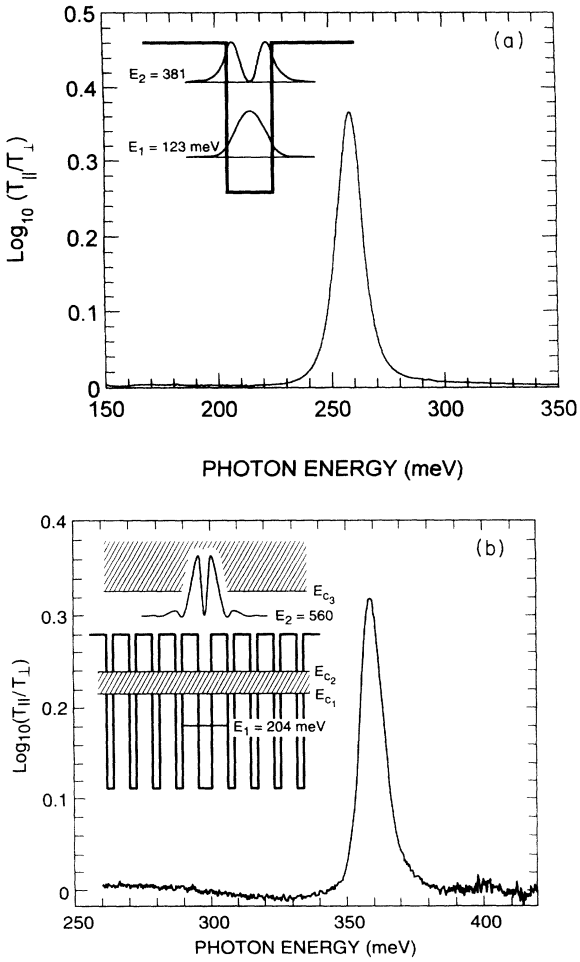

FIG. 4. Measured absorbance, at $T = 10$ K, and band diagram of bound-to-bound transitions in symmetric well structures. (a) Single quantum well; sample parameters: well width 52 Å, sheet density $\rho_s = 2.5 \times 10^{11}$ cm^{-2}, number of periods $N = 20$, number of passes $n_p = 8$. (b) Bragg confined quantum well; sample parameters: central well width 32 Å, $\lambda/4$ barrier 39 Å, $\lambda/4$ well 16 Å, $\rho_s = 3.4 \times 10^{11}$ cm^{-2}, $N = 20$, $n_p = 6$.

further confirms the expectation that the integrated absorption only depends on the properties of the ground state.

While the first factor in (27) decreases linearly with the inverse of the ground-state energy, the dependence of the kinetic factor on the considered quantum well structure is less evident. In order to clarify to which extent the kinetic factor can vary in different structures, we have reported in Fig. 3 the dependence of the sum rule on the ground-state energy for three different structures, namely, a single, a double, and a triple quantum well. For the last three structures the ground-state energy was changed only by varying the width of the thickest well. The parameters of these structures are reported in the captions of Figs. 4 and 5. The choice of the ground-state energy as the independent variable implies that any difference in the results of Fig. 3 must be attributed to the kinetic factor. In particular, it turns out that this factor is more effective (stronger reduction) in a single-quantum-well structure and that its contribution may even increase for increasing energies, as in the case of the triple quantum well. This is clearly at variance with the naive expectation that the kinetic energy increases for increasing total confinement energy.

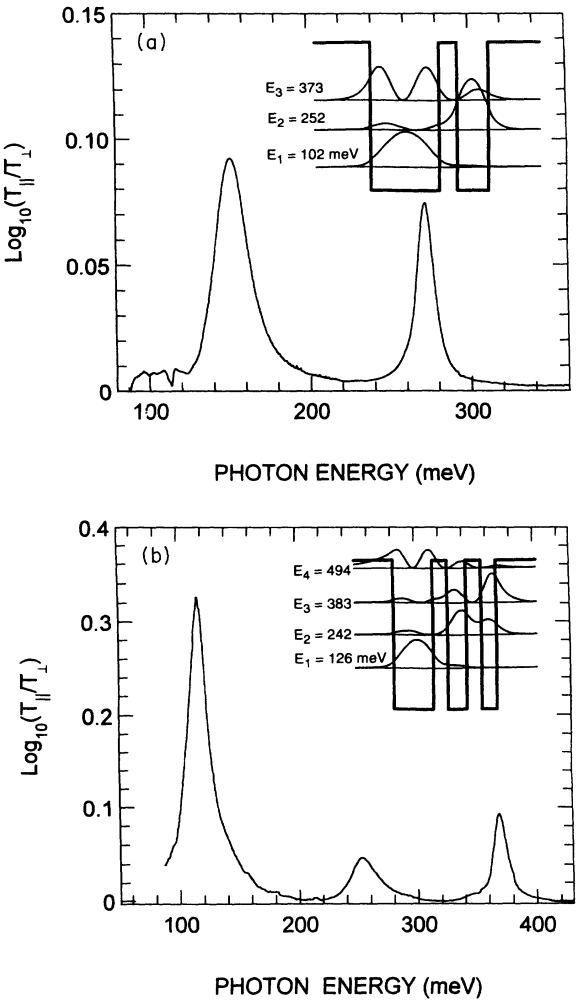

FIG. 5. Measured absorbance, at 10 K, and band diagram of bound-to-bound transitions in asymmetric coupled quantum well structures. (a) Two-coupled well; sample parameters: thick well 59 Å, coupling barrier 13 Å, thin well 24 Å, sheet density $\rho_s = 1.2\times10^{11}$ cm^{-2}, number of periods $N = 20$, number of passes $n_p = 8$. (b) Three-coupled well; sample parameters: well widths, looking at the inset from left to right, 46 Å, 20 Å, 19 Å, coupling barriers 10 Å, $\rho_s = 3.2 \times 10^{11}$ cm^{-2}, $N = 40$, $n_p = 8$.

V. EXPERIMENTAL RESULTS

The most natural and direct way to measure the oscillator strength of optical transitions is by means of absorption experiments.[30] In the first part of this section we will show how the oscillator strength is related to the area under the absorption peak; we will then compare the experimental results with the theory for various structures, trying to encompass the most significant cases concerning intersubband transitions in bounded systems. At the end we will present data, associated with an appropriately designed heterostructure, showing unmistakable evidence of a sum rule which is in excellent agreement with our theoretical calculations.

The absorption spectra were measured with a Nicolet 800 Fourier-transform infrared (FTIR) spectrometer. The samples were mounted in a liquid-helium flow cryostat, where the temperature can be varied between 5 and 300 K. Only the component normal to the layers of the electric field of the incident wave significantly contributes to intersubband transitions. Thus in order to increase the net absorption we fabricate a multipass waveguide by cleaving a bar and polishing both cleaved ends at a 45° angle. One of these edges was then illuminated at normal incidence. To obtain a very flat base line, our spectra were taken following a three-step procedure. (1) We measure the ratio of the absorbance between the polarization in the plane of the layers and the polarization normal to the plane of the layers, $\log_{10}(T_{\|}/T_{\perp})$, to remove instrumental, substrate, and free carrier contributions to the absorption; (2) we repeat the same measurement without the sample in the cryostat to determine the spectral dependence of $\log_{10}(T_{\|}/T_{\perp})$ due to the many optical components (mirrors, windows, beam splitters) in the FTIR, which may have different dispersion for S or P polarization; (3) we subtract the spectrum of point (2) from the spectrum of point (1) minimizing then all the contributions which do not come from the quantum wells. Special care has to be taken also to avoid any ellipticity of the light typically introduced by the off-axes parabola mirrors. To reduce this effect we use two polarizers, one before and one after the sample. It is easy to show that the absorption coefficient of the quantum wells is related to the absorbance by

$$\alpha_W = \frac{\ln(10)\log_{10}(T_{\|}/T_{\perp})}{L_{\text{int}}} , \tag{28}$$

where L_{int} is the total interaction length in the quantum wells defined as

$$L_{\text{int}} = \frac{L_W N n_p}{\cos\theta} , \tag{29}$$

where L_W is the total quantum well thickness plus that of the thin coupling barriers, N is the number of periods, n_p the number of passes, and θ the angle of incidence with respect to the normal to the plane of the layers (45° in our case). The area under the absorption peak corresponding to the $0 \rightarrow j$ intersubband transition multiplied by ln(10) is the integrated absorption strength I_A. The latter is given, in eV units, by

$$I_A = \frac{\pi\hbar\rho_s N n_p e}{2m_0\varepsilon_0 cn} \frac{\sin^2\theta}{\cos\theta} f_{0j} , \tag{30}$$

where ρ_s is the sheet electron density in the wells, $n = 3.34$ is the refractive index, m_0 is the electron mass, and c is the velocity of light in a vacuum.[31,32] Thus from the integrated absorption strength and the knowledge of the other quantities in Eq. (30), one can deduce the oscillator strength f_{0j} of the transition.

Our AlInAs/GaInAs structures, grown lattice matched to a semi-insulating (100)InP substrate, consist of several periods (from 20 to 40). In order to avoid any superlattice effect each period is separated from the others by thick undoped AlInAs barriers, typically 200 Å. All the structures are doped n-type with silicon in the wells; in the case of multiple quantum wells only the thickest well of the period is doped. The doping concentration, varying between 2×10^{17} and 1×10^{18} cm^{-3}, is always such that the Fermi energy E_f lies well below any excited level; all the observable transitions at low temperature are then the ones from ground to excited states. All structures are provided with n^+ 4000 Å cladding layers which can be used as contacts if an electric field has to be applied. More details on the individual structures are given in the figure captions.

Figures 4–6 show the measured absorbance (= −log[transmission]) spectra, at cryogenic temperature ($T = 5$ K), for three different classes of structures. Figures 4(a) and 4(b) display spectra of transitions for symmetric potential wells. Figure 4(a) is the spectrum of a single quantum well where the transition arises between bound states below the barrier height. In Fig. 4(b) the confinement of the excited state is achieved using two high reflectivity quarter-wave stacks for the de Broglie electron wavelength corresponding to the energy of the first transmission resonance above the quantum well. The physical mechanism providing the high reflectivity necessary for the localization of the wave functions is constructive interference of the waves partially reflected by the interfaces of the stacks.[33,34] Figures 5(a) and 5(b) exhibit a different class of transitions. In this case the structures are asymmetric and the separation between the centers of charge of the wave functions, for some transitions, can be comparable to the extension of the wave function itself (40–50 Å). One can easily see, looking, for instance, at the band diagram of Fig. 5(a), that the first and third states are essentially confined by the thick well while the second is approximately confined by the thin well. Similarly for the structure of Fig. 5(b), the first and the fourth states belong to the largest well while the second and third are localized in the thinner wells. For this potential, all transitions are allowed since the parity of the wave functions is broken by the asymmetry. Thanks to this property, these asymmetric coupled wells have been recently studied as nonlinear optical materials in the mid-infrared.[35–37] Figure 6 shows the absorption spectrum for bound-to-continuum transitions. In this case the well width has been reduced in order to obtain only one bound state in the quantum well. The transitions occur between the confined state and the extended states in the continuum. Here the shape of the peak is primarily controlled by (1) the value of the transition matrix elements between the ground and the scattering states and (2) the density of states in the continuum part of the spectrum. The broadening mechanism (impurity scattering, interface roughness, etc.) are still present but they are effecting the spectrum solely by reducing the sharpness of some features such as, for instance, the cutoff at energy $h\nu = \Delta E_c - E_1$ where the peak begins to rise.

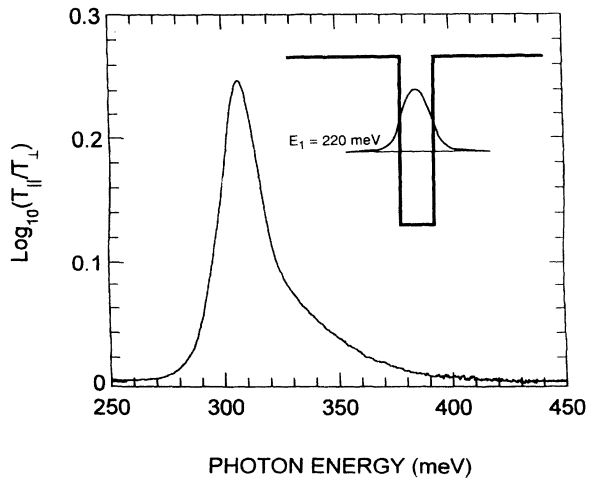

FIG. 6. Measured absorbance, at 10 K, and band diagram of bound-to-continuum transitions in a potential well; sample parameters: well width 30 Å, sheet density $\rho_s = 3 \times 10^{11}$ cm^{-2}, number of periods $N = 40$, number of passes $n_p = 6$.

In Sec. III we derived an expression for the momentum matrix element $\langle P\rangle_{0j} = \langle\psi^{(0)}|P|\psi^{(j)}\rangle$ [Eq. (8)] associated with a single transition from the ground state to the jth state. It is important to remark that, even though we still are in a three-band model, the result is only dependent on the conduction component ϕ_c, which comes from the solution of the differential equation (2) together with the correct normalization given by (12). This is a salient and very operative result which allows us to calculate the oscillator strength in a three-band model only in terms of the conduction component. Equation (8) also clarifies the dependence of the intersubband transitions on the nonparabolic effective mass. This gets in the formula at the denominator, as reduced mass of the ground and final state, appropriately weighted by the wave functions in the wells and in the barriers.

As discussed in the previous sections, the standard procedure to evaluate matrix elements for intersubband

transitions in the presence of nonparabolicity is based on an ill-defined dipole operator. We have instead shown that the correct expression for the dipole operator in the presence of nonparabolicity must account for the effects due to the nonvanishing valence components of the total wave function. In spite of the fact that in our formalism the matrix elements are more easily computed using the momentum operator, due to the widespread use of the dipole-matrix elements in the literature, we prefer to report, beside the oscillator strengths, the dipole moment $\langle Z\rangle_{0j}$ of a given transition, as deduced from the commutation relation (10). It will then be easier to compare these results with previous reports. The experimental and theoretical values of $|\langle Z\rangle_{01}|$ are quoted in Table I.

We are now in the position to comment about the total oscillator strength related to these structures. First it is important to notice that for intersubband transitions the oscillator strength decays very rapidly with increasing energy (e.g. $f_{0i} \sim E_{0i}^{-3}$ for a square well). For this reason the measurable absorption peaks, where 95% or more of the oscillator strength is contained, are all concentrated in a short spectral range, at most of the order of the band discontinuity between the two components ($\simeq$ 500 meV in our material).

Our data cover the entire spectral range, measuring all the relevant transitions from the ground to the accessible states. This is a remarkable difference between these data and those for interband transitions, where data refer to a specific subset of the spectrum,[38–40] and the sum rules are verified only as normalized value to the examined range. To be more accurate we have to make clear that, for those structures where the transitions occur among bound states (Figs. 4 and 5), in fact a small portion of the oscillator strength is involved in transitions to the continuum. However, this quantity never exceeds 2% of the total oscillator strength and, being below the sensitivity of the measurement, is within our experimental error.

Obviously the total oscillator strength is proportional to the sum of all the areas under the absorption peaks of the spectrum. In the case of bound transitions we estimated the areas fitting the peaks with Lorentzian line shapes, while for bound-to-continuum transitions we simply took the value of the integral under the curve directly from the data, without any particular fitting procedure. In Table I we give a comparison between experimental results and the results of our model using formulas (6), (9), and (27), respectively, for the oscillator strength, the dipole matrix element, and the sum rule. As one can easily see from Eq. (27), the sum rule for intersubband transitions is not a constant, depending upon the properties of the conduction-band component of the ground state. It is clearly shown in Fig. 3 that this dependence is also a function of the kinetic energy of the ground state. So given two different potentials, exhibiting completely different absorption spectra, they will have the same value of the total oscillator strength only if their ground states are identical both in energy and shape. This condition, which is in principle impossible to satisfy using two different structures, is indeed realizable applying an electric field to a suitably designed heterostructure where varying the field we can observe dramatic changes of the absorption spectra due to modifications of the excited states. However, since the ground state is not significantly altered, the sum rule ensures the conservation of the integrated absorption in the presence of the field. This result was experimentally demonstrated using an AlInAs/GaInAs heterostructure like the ones described above (more details about this structure are given in the caption of Fig. 7). We measured electronic intersubband transitions in thin quantum wells sandwiched between a $\lambda/4$ reflector barrier and a conventional rectangular barrier. Quantum confinement of the first resonance above the well is obtained in the presence of a strong electric field of the appropriate polarity. This produces a dramatic narrowing of the spectrum; in the opposite bias polarity, the latter is instead strongly broadened.

Figure 7(a) shows the conduction-band diagram of a portion of this structure at zero bias. Indicated are the energy levels and the modulus squared of the wave functions. From the shape and spatial extension of the $|\psi|^2$'s one sees that the first continuum resonances shown in Fig. 7(a) represent, from a physical point of view, quasibound states at energies above the barrier of the doped well plus thick barrier combined. They are spatially confined to this region by the AlInAs/GaInAs ultrathin layers which act essentially as high reflectivity ($\geq$ 0.90) quarter-wave electron stacks in the energy range from 0.52 eV (top of the barrier) to 0.64 eV measured from the bottom of the well. These multilayer barriers were designed in order to be high reflectivity electron mirrors also in the presence of electric fields ($0 \leq F \leq 4.8 \times 10^4$ V/cm). This ensures that the first continuum resonance does not appreciably penetrate in the region to the left of the thick well in Fig. 4, when a bias is applied.

At zero bias the absorption spectrum includes mainly

TABLE I. Experimental and theoretical values of the total oscillator strength $f_{\rm tot}$, of sum rule (SR), Eq. (27), and of the oscillator strength f_{01} of the strongest transition, in five different quantum well structures; the parameters of the five structures are given in the text or in the corresponding figure captions.

	$f_{\rm tot}^{\rm (exp)}$	$f_{\rm tot}^{\rm (th)}$	SR	$f_{01}^{\rm (exp)}$	$f_{01}^{\rm (th)}$	$\langle Z\rangle_{01}^{\rm (exp)}$ (Å)	$\langle Z\rangle_{01}^{\rm (th)}$ (Å)
Single QW	15.8	14.8	13.8	15.8	14.8	15.3	14.8
Double QW	15.4	16.1	15.3	10.7	10.8	16.4	16.5
Triple QW	14.1	15.9	15.0	10.5	10.3	18.6	18.4
Bragg QW		13.3	12.0	9.6	9.7	10.1	10.2
QWIP	11.3	12.3	11.5				

the transitions from the ground state to the first three resonances in the continuum (states 3, 4, and 5 in our notation, state 5 is not indicated in Fig. 7). Because of the close spacings of the latter the spectrum is broadened into a band. As the field is raised, for positive polarity [Fig. 7(b)] the localization of the first resonance above the center well is increased. This has the effect of enhancing the matrix element of the $0 \rightarrow 3$ transition and hence the corresponding oscillator strength f_{03} and absorption coefficient. An opposite effect occurs for the second continuum resonance, which becomes increasingly localized in the barrier, thus reducing the spatial overlap with the ground state and therefore also the oscillator strength. This is similar to the behavior of the ground and first excited states of a rectangular well in an electric field. The centers of charge distributions for the two states are shifted in opposite directions by the electric field. In summary, an increase of the electric field in the positive polarity should lead to greatly enhanced absorption for the $0 \rightarrow 3$ transition and strongly decreased absorption for the $0 \rightarrow 4$ and $0 \rightarrow 5$ transitions, producing an overall narrowing of the spectrum. In the opposite bias polarity instead there is negligible overlap between the resonances, now localized in the AlInAs barrier, and the ground state. The absorption spectrum is then controlled by transitions to extended states at energies above the barrier and is therefore expected to be broad.

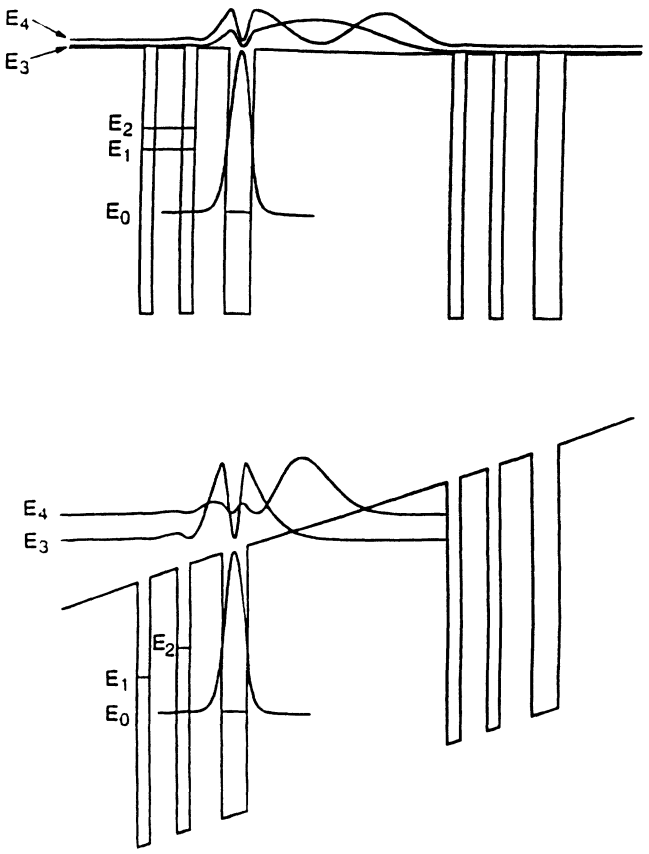

FIG. 7. (a) Energy band diagram of the structure showing the calculated energy levels and the modulus squared of some of the corresponding wave functions (E_0 = 204 meV, E_1 = 310 meV, E_2 = 351 meV, E_3 = 511 meV, E_4 = 520 meV). The thickness of the widest GaInAs well is 34 Å. The $\lambda/4$ stack on the left of this well comprises two 17 Å thick GaInAs wells and two AlInAs barriers, 36 Å and 42 Å, respectively. Each period is repeated 40 times (number of periods $N = 40$). The thickness of the barrier on the right of the 34 Å well is 270 Å. (b) Energy band diagram of the structure in a strong electric field (4.8×10^4 V/cm, positive bias polarity). Indicated are the calculated energy levels and the modulus squared of some of the corresponding wave functions. Note that the first continuum resonance (E_3) has been strongly localized above the well while the second one (E_4) has been mostly confined to the barrier.

The absorption spectra of Fig. 8, taken at different electric fields, confirm the above physical picture. At negative bias the spectrum is very broad, while for positive bias it narrows with increasing field. A more detailed study of the spectra is reported in Fig. 9, where the areas under the absorption curves is plotted versus applied field. From these data one acknowledges the independence of the integrated absorption on the electric field within the experimental error (8%). There are also other transitions: those from the ground state of the thick well to the confined states of the $\lambda/4$ stack, i.e., the energy levels E_1 and E_2 [Figs. 7(a) and 7(b)], which are not included in the measured integrated absorption strength obtained from the area under the peaks of Fig. 8. These transitions have a small oscillator strength ($\sim$ 6% on each) because of their diagonal nature in real space and are not observed in our spectra. However, the contribution of these transitions to the total integrated absorption

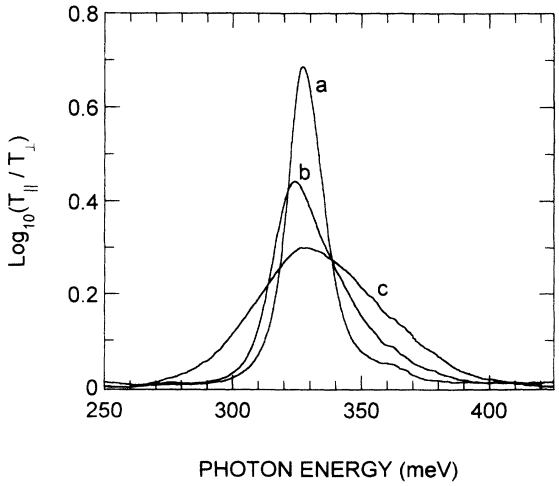

FIG. 8. Absorption spectra at 10 K taken for various bias conditions: (a) 4.8×10^4 V/cm; (b) 1.2×10^4 V/cm; (c) -3.6×10^4 V/cm. The positions of the peak, for positive polarity, are in good agreement with the calculated energy differences ($E_3 - E_0$ = 316 meV at 1.2×10^4 V/cm; $E_3 - E_0$ = 332 meV at 4.8×10^4 V/cm). In the opposite polarity the absorption is peaked near the onset of the continuum ($\Delta E_c - E_0$) and is broadened towards lower energies by tunneling effects.

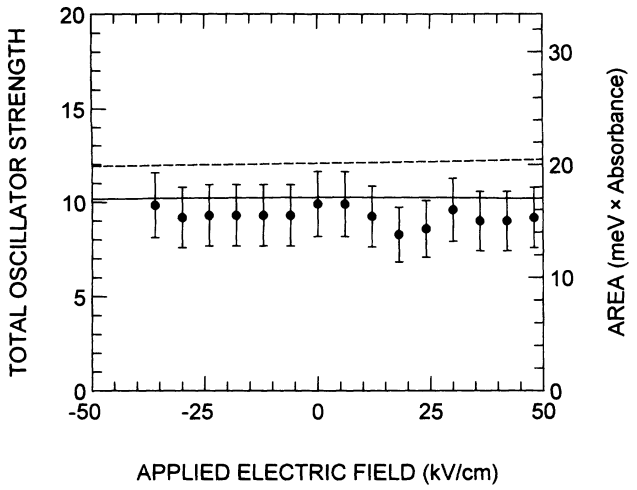

FIG. 9. Measured integrated absorption as a function of the electric field (dots). On the right y axis the value of the areas are reported, as measured from the spectra, in units of (meV×absorbance). On the left y axis the areas are converted in oscillator strength following Eq. (30); on the axis it is possible to compare the data with the results predicted by the sum rule. The dashed line is the sum rule calculated from Eq. (27); the solid line represents the sum rule minus the amount of oscillator strength involved in the transition from the ground state to the energy levels E_1 and E_2 in Fig. 7.

is not negligible. In Fig. 9 we display the total oscillator strength (dashed line), calculated using the sum rule (27). As we were expecting this is almost a constant as a function of the electric field, varying by 3% within a bias range of 100 kV/cm. Nevertheless, the comparison with the experiment is not satisfactory. We can attain better agreement if we subtract from the total oscillator strength the amount of it "lost" in the diagonal transitions (solid line). Notice that this correction does not affect the conservation of the integrated absorption in the range of the observed transitions. Actually for this quantity the variation across the range of applied electric field is even reduced below 1%.

In this structure the electric field significantly modifies high energy states and almost does not affect the ground state. This effect is the opposite of the one we would expect when an electric field is applied to wide quantum wells, which basically alters only the states at low energy closer to the bottom of the well. To understand the peculiar behavior of our structure we have to remember that the states which are more perturbed by an electric field are those closer to the band edge. The singular design of our potential sets the ground state at almost 200 meV from the bottom of the well whereas the excited states, i.e., the continuum resonances, extend mainly above the thick barrier at a very close energy from the top (Fig. 7). When an electric field bends the band edge, it immediately modifies the excited states in the continuum letting almost unperturbed the states confined in the thin well.

VI. CONCLUSIONS

We have derived a compact formula for the sum of the oscillator strengths for intersubband transitions. This formula, which is an appropriate average performed on the ground state, takes into account the effects of nonparabolicity and different effective masses in the well and barrier materials. The analysis, based on the envelope-function formalism in the Kane approximation, has been supported by experimental results in a number of differently shaped quantum well structures. The main consequence of nonparabolicity has been shown to be an overall reduction of the oscillator strengths which can be half of the value m_0/m^* predicted in the parabolic case. The dependence of the sum rule on the specific quantum well shape has been analyzed in few illustrative cases, and one of its consequences, namely the invariance of the integrated absorption strength upon application of a weak external electric field, has been verified experimentally.

ACKNOWLEDGMENTS

We acknowledge the precious collaboration of D.L. Sivco and A.Y. Cho in the growth of the structures, and we thank G.A. Baraff for the careful reading of the manuscript.

APPENDIX

We start by defining the new valence components ϕ_v and $\phi_{v'}$ through the unitary transformation

$$\begin{aligned} \phi_v &= \sqrt{\tfrac{2}{3}}\phi_{\rm lh} - \sqrt{\tfrac{1}{3}}\phi_{\rm so} , \\ \phi_{v'} &= \sqrt{\tfrac{1}{3}}\phi_{\rm lh} + \sqrt{\tfrac{2}{3}}\phi_{\rm so} . \end{aligned} \tag{A1}$$

It is readily seen that the transformed 3×3 Hamiltonian acting on the vector $(\phi_c, \phi_v, \phi_{v'})$ can be expressed as

$$\mathcal{H} = \begin{pmatrix} E_c & \frac{p_{cv}}{m_0}p_z & 0 \\ -\frac{p_{cv}}{m_0}p_z & E_v & \Delta \\ 0 & \Delta & E_{v'} \end{pmatrix} . \tag{A2}$$

It can be easily seen from the third row of (A2) that $|\phi_{v'}| = \Delta/(E - E_{v'})|\phi_v| \le \Delta/(E_c - E_{v'})|\phi_v|$. Since the contribution of $\phi_{v'}$ to the second row of (A2) is given by $\Delta\phi_{v'}$, we can immediately observe that this contribution is a factor of $\Delta^2/(E_c - E_{v'})(E_c - E_v) \simeq \Delta^2/(\bar{E}_v - E_c)^2$ smaller than other terms of the same row, where $\bar{E}_v$ is the average of the valence-band energies. The same conclusion can be reached for the normalization of the total wave function, where $\phi_{v'}$ contributes with a term which is a factor of $[\Delta/(E_c - \bar{E}_v)]^2$ smaller than the contribution of ϕ_v. For typical III-V semiconductors this factor is quite small. In GaInAs, for example, we have

$[\Delta/(E_c - \bar{E}_v)]^2 \simeq 0.04$.[19] We can thus neglect the presence of $\phi_{v'}$ and consider the reduced 2×2 Hamiltonian (4) acting on the two-dimensional vector (ϕ_c, ϕ_v).

As for optical transitions, it is readily seen that the unitary transformation (A1) gives the new momentum matrix

$$\mathcal{P} = \begin{pmatrix} 0 & p_{cv} & 0 \\ -p_{cv} & 0 & 0 \\ 0 & 0 & 0 \end{pmatrix} . \tag{A3}$$

Therefore the $\phi_{v'}$ component does not contribute to optical transitions.

[1] *Intersubband Transitions in Quantum Wells*, edited by E. Rosencher and B. Levine (Plenum, New York, 1992).

[2] F. Capasso, C. Sirtori, and A.Y. Cho, IEEE J. Quantum Electron. **QE-30**, 1313 (1994).

[3] J. Faist, F. Capasso, D.L. Sivco, C. Sirtori, A.L. Hutchinson, and A.Y. Cho, Science **264**, 553 (1994).

[4] H. Asai and Y. Kawamura, Appl. Phys. Lett. **56**, 746 (1990).

[5] B.F. Levine, A.Y. Cho, J. Walker, R.J. Malik, D.A. Kleinman, and D.L. Sivco, Appl. Phys. Lett. **52**, 1481 (1988).

[6] J.L. Pan, L.C. West, S.J. Walker, R.J. Malik, and J.F. Walker, Appl. Phys. Lett. **57**, 366 (1990).

[7] H.C. Chui, S.M. Lord, E. Martinet, M.M. Fejer, and J.S. Harris, Jr., Appl. Phys. Lett. **63**, 364 (1993).

[8] G. Bastard, *Wave Mechanics Applied to Semiconductor Heterostructures* (Les Editions de Physique, Les Ulis, France, 1988).

[9] D. F. Nelson, R. C. Miller, and D. A. Kleinmann, Phys. Rev. B **35**, 7770 (1987).

[10] R.P. Leavitt, Phys. Rev. B **44**, 11 270 (1991).

[11] A. Sommerfeld and H. Bethe, in *Elektronentheorie der Metalle,* edited by H. Geiger and K. Scheel, Handbuch der Physik Vol. 24/2, (Springer, Berlin, 1933); see also A.H. Wilson, *The Theory of Metals* (Cambridge University Press, Cambridge, 1936), p. 49.

[12] M. Lax, in *Photoconductivity Conference,* edited by R.G. Breckenridge (Wiley, New York, 1956), p. 111.

[13] L.I. Schiff, *Quantum Mechanics* (McGraw-Hill, New York, 1968), p. 21.

[14] T. Hiroshima and R. Lang, Appl. Phys. Lett. **49**, 456 (1986).

[15] A. Persson and R.M. Cohen, Phys. Rev. B **38**, 5568 (1988).

[16] U. Ekenberg, Phys. Rev. B **40**, 7714 (1989).

[17] K.H. Yoo, L.R. Ram-Mohan, and D.F. Nelson, Phys. Rev. B **39**, 12 808 (1989).

[18] *Intrinsic Properties of Group IV Elements and III-V, II-VI, and I-VII Compounds,* Landolt-Börnstein, New Series, Group 3, Vol. 22, Pt. a (Springer-Verlag, Berlin, 1987).

[19] G. Bastard, Phys. Rev. B **25**, 7584 (1982).

[20] M. Altarelli, in *Heterojunctions and Semiconductor Heterostructures,* edited by G. Allan, G. Bastard, N. Boccara, M. Lannoo, and M. Voos (Springer-Verlag, Berlin, 1986).

[21] E. Rosencher and Ph. Bois, Phys. Rev. B **44**, 11 315 (1991).

[22] See, for instance, H.A. Bethe and E.E. Salpeter, *Quantum Mechanics of One- and Two-Electron Atoms* (Springer-Verlag, Berlin, 1957).

[23] D.Y. Smith and D.L. Dexter, in *Progress in Optics,* edited by E. Wolf (North-Holland, Amsterdam, 1972), Vol. 10.

[24] F.M. Peeters, A. Matulis, M. Helm, T. Fromherz, and W. Hilber, Phys. Rev. B **48**, 12 008 (1993).

[25] D.P. Davé and H.F. Taylor, Phys. Lett. A **184**, 301 (1994).

[26] F. Seitz, *Modern Theory of Solids* (McGraw-Hill, New York, 1940) p. 644.

[27] E.O. Kane and E.I. Blount, in *Tunneling Phenomena in Solids,* edited by E. Burnstein and S. Lundqvist (Plenum, New York, 1969); R. Beresford, Semicond. Sci. Technol. **8**, 1957 (1993).

[28] J.S. Levinger, M.L. Rustgi, and K. Okamoto, Phys. Rev. **106**, 1191 (1957).

[29] Perfect specular alignment would be obtained only if the conduction-band offset between well (w) and barrier (b) materials were given by $\Delta E_c = [E_{\rm gap}(b) - E_{\rm gap}(w)]/2$, with $E_{\rm gap} = E_c - E_v$.

[30] D.A.B. Miller, J.W. Weiner, and D.S. Chemla, IEEE J. Quantum Electron. **QE-22**, 1816 (1986).

[31] C. Sirtori, F. Capasso, D.L. Sivco, S.N.G. Chu, and A.Y. Cho, Appl. Phys. Lett. **59**, 2302 (1991).

[32] B.F. Levine, R.J. Malik, J. Walker, K.K. Choi, C.G. Bethea, D.A. Kleinmann, and J.M. Vanderberg, Appl. Phys. Lett. **50**, 273 (1987).

[33] C. Sirtori, F. Capasso, J, Faist, D.L. Sivco, S.N.G. Chu, and A.Y. Cho, Appl. Phys. Lett. **61**, 898 (1992).

[34] F. Capasso, C. Sirtori, D.L. Sivco, S.N.G. Chu, and A.Y. Cho, Nature (London) **358**, 565 (1992).

[35] C. Sirtori, F. Capasso, D.L. Sivco, A.L. Hutchinson, and A.Y. Cho, Appl. Phys. Lett. **60**, 151 (1992).

[36] C. Sirtori, F. Capasso, D.L. Sivco, and A.Y. Cho, Phys. Rev. Lett. **68**, 1010 (1992).

[37] C. Sirtori, F. Capasso, D.L. Sivco, and A.Y. Cho, Appl. Phys. Lett. **60**, 2678 (1992).

[38] M. Whitehead, G. Parry, K. Woodbridge, P.J. Dobson, and G. Duggan, Appl. Phys. Lett. **52**, 345 (1988).

[39] A.J. Moseley, D.J. Robbins, A.C. Marshall, M.Q. Kearly, and J.I. Davis, Semicond. Sci. Technol. **4**, 184 (1989).

[40] C. Sirtori, J. Faist, F. Capasso, D.L. Sivco, and A.Y. Cho, Appl. Phys. Lett. **62**, 1931 (1993).